Statistical evidence of a seismic quiescence before the M_w 8.1 Iquique earthquake, Chile

F. Aden-Antoniów[1,2], C. Satriano[2], P. Bernard[2], N. Poiata[2], E-M. Aissaoui[2], J-P. Vilotte[2], W.B. Frank[1,3]

[1] Department of Earth Sciences, University of Southern California, Los Angeles, CA, USA
[2]Institut de Physique du Globe de Paris, France
[3]Department of Earth, Atmospheric and Planetary Sciences, Massachusetts Institute of Technology, Cambridge, MA, USA

Key Points:

- Iquique earthquake preparatory phase;
- Kolmogorov-Smirnov test applied to the background-seismicity rate;
- Quiescence before great earthquakes;

Corresponding author: Florent Aden-Antoniow, adenanto@usc.edu

Abstract

The 2014 Iquique seismic crisis (Chile), culminating with a M_w 8.1 earthquake, April 1st, highlights a complex unlocking of the North Chile subduction interface which has been considered as a seismic gap since 1877. During the year preceding this event, at least three seismic clusters were observed: in July 2013 and January and March 2014. These clusters possibly indicate aseismic slip transients accompanying the progressive destabilization of the plate contact. Recent studies have proposed large-scale slab deformation as a potential trigger for the megathrust earthquake. However, no evidence of gradual unlocking of the interface or transient deformation has yet been found in the seismic rate. To address this question, we develop a dense earthquake catalog during the fifteen months preceding the mainshock from the continuous waveform dataset recorded by the Integrated Plate Boundary Observatory Chile (IPOC) and Iquique Local Network (ILN) networks. After declustering the seismicity, a space-time analysis highlights a large-scale acceleration of the seismicity along the interface while it decelerates at intermediate-depths. We then demonstrate the existence of a seismic quiescence down-dip of the mainshock rupture before the July 2013 cluster. We propose that this seismic quiescence is related to fluid circulation and/or aseismic motion along upper-plate crustal fault(s).

1 Introduction

Chile is well known for its intense seismic activity across the country where the largest earthquake ever was recorded in Valdivia in 1960 (M_w 9.5). more recently there has been a series of major events, i.e. the M_w 8.8 Maule earthquake in 2010 (e.g. Delouis et al., 2010; Vigny et al., 2011). The northern portion of the Chilean subduction, from the city of Arica (-18.5N) to the Mejillones peninsula (-23N), has been spared from great earthquakes since 1877 (Nishenko, 1991; Comte & Pardo, 1991), and is considered a seismic gap. On April 1st 2014, the Iquique earthquake of moment magnitude 8.2 broke a section of this gap with a maximum slip of about 8 m (Lay et al., 2014; Ruiz et al., 2014; Yagi et al., 2014; Meng et al., 2015; Duputel et al., 2015; Liu et al., 2015; Jara et al., 2018). This earthquake was preceded by a series of seismic-swarms described by Schurr et al. (2014): the very first anomalous and shallow activity was reported on July 23rd 2013 offshore the city of Iquique and lasted for few days; the second swarm appeared southward during the first days of January 2014; the last swarm happened on March 16th 2014 and started with a major upper-plate crustal foreshock of M_w 6.7 (Bedford et al., 2015) and lasted until the mainshock of April 1st. Ruiz et al. (2014) proposed that the last cluster of March 2014 was driven by a slow-slip event along the interface. Kato et al. (2016) detected several repeating earthquake since July 2013 suggesting that each episodic swarm was driven by slow-slip, ultimately leading to the nucleation of the Iquique earthquake. Socquet et al. (2017) found evidence of these preparatory aseismic signals in the GPS data.

The unlocking of the interface by slow-slip events prior to major earthquakes has been observed at multiple subduction zones. Examples include the Tohoku-oki earthquake (Kato et al., 2012), the Arequipa earthquake (Ruegg et al., 2001), the Illapel earthquake (Huang & Meng, 2018; Poli et al., 2017), and more recently the Valparaiso sequence in April 2017 (Ruiz et al., 2017). Bouchon et al. (2013) observed a synchronization of high seismic moment release at both shallow (depth<40km) and deeper (depth>80km) portions of the subduction during the three seismic swarms and interpreted it as as a deformation within the slab. Additionally, the slab-pull Tarapaca earthquake (M_w 7.1), which occurred in 2005 on an inherited normal fault at the latitude of Iquique (Peyrat et al., 2006), altered the plate motions and seismic behavior of the area, as demonstrated by Jara et al. (2017). The authors suggest a preparatory phase even longer than previously expected, comparable to the decadal time scale of the 2011 Tohoku-oki earthquake preparatory phase (Mavrommatis et al., 2014; Yokota & Koketsu, 2015), and more generally to subduction earthquakes through the initiation of stable slip (Bouchon et al., 2013).

Despite the important results concerning the preparatory phase of the Iquique earthquake, the potential of the IPOC (GFZ CNRS-INSU, 2006) and ILN (Cesca et al., 2009) networks have not yet fully been exploited to study the seismicity during the months preceding the Iquique earthquake. The CSN catalog contains 2-3 events per day (with a completeness magnitude of 4 (Jara et al., 2017)). A visual inspection of the data, however, shows numerous undetected events. The objective of this work is to build a richer catalog to home in on the micro-seismicity in order to statistically highlight in time and space transients that could be involved in the preparatory phase of the earthquake. With this work we aim to precisely identify areas where aseismic slip could have played a role in the nucleation of the mainshock.

2 Building the catalog: detection, location and event selection

The IPOC network was deployed in 2006 just before the M$_w$ 7.7 Tocopilla earthquake (2007) in order to study the seismic gap of northern-Chile. It was designed to capture a large range of deformation processes by using seismometers, strong-motion sensors, GPS, magnetotelluric sensors, creepmeters and tiltmeters. This network represents a unique opportunity for studying the Northern-Chilean subduction seismicity: 16 stations with a dense distribution close to the trench to investigate in detail both interface and intraplate seismicity.

We built a new catalog following the method described in Ruiz et al. (2017). It combines automated methodologies to detect and locate seismic events. Our catalog spans from December 13th 2012 to March 31st 2014. For the detection procedure we selected 7 stations (Figure 1) which remained operational over the largest period before the Iquique earthquake. We obtained a first set of detections with the BackTrackBB method (Poiata et al., 2016, 2018) applied to the vertical components associated with a P-wave velocity model. This method builds kurtosis-based characteristic functions from the signal at different frequency bands in order to include time-frequency features. The cross-correlation of each pair of characteristic functions is then backprojected into 3D time-delay grid. The detection of a seismic event is declared if the maximum of the stack of all time-delay grid - also called the source location function (SLF) - overcomes a threshold value chosen by the operator. Here we used 10 frequency bands between 5 and 50 Hz. During this preliminary detection step, we normalized the SLF to 1 and arbitrary put it at a power 18. This significantly reduces the scattering of the SLF when there is a seismic source in the window of analysis and allows us to use the size of its 3D error-ellipsoid as a detection-trigger parameter (100km semi-axis) (See Figure S1 in Supplementary Information). When there is no coherent seismic sources observed in the data, the SLF remains scattered which means a larger 3D error-ellipsoid (See Figure S2 in Supplementary Information). This step greatly improves the number of detected events with low signal to noise ratio; however, it also implies many false detection that need to be removed later in the process. In a second step, we used as many stations as available and were able to differentiate P and S waves with a polarization analysis based on a singular value decomposition following Rosenberger (2010) (See Figure S3 in Supplementary Information). In order to improve the location of the detected events, we relocate these events anew with BackTrackBB applied to the three components (See Figure S4 in Supplementary Information).

To locate earthquakes we use a 1D velocity model proposed by Dorbath et al. (2008). To properly recover the geometry of the subduction at these latitudes, we incorporated the slab following the geometrical model of SLAB1.0 (Hayes et al., 2012) with velocities following a 3D velocity model (Dorbath et al., 2008). We finally relocate every detection with the NonLinLoc program (Lomax et al., 2000; Lomax, 2005) in order to obtain a probability density of location, allowing us to select/discard events according to the size of their 68% error ellipsoid. As the velocity model used here is poorly resolved at depth, we will consider the 3D-ellipsoid projected on the horizontal plane.

We obtained a total of 62054 detections using BackTrackBB and discarded events which have a 2D-ellipsoid with semi-axes length greater than 10km. This threshold represents the compromise between the number of events kept and the maximum length of the 2D ellipsoid (See Figure S4 and S5 in Supplementary Information). We kept 35371 earthquakes between -22.5 N and -18.5 N and between -72 E and -66 E. As a comparison, 3503 events are in the CSN catalog for the same period and the same area. We lowered the completeness magnitude from 4.0 for the CSN to 2.6 (Figure 1b).

With the aim of studying the spatio-temporal variations of the seismicity we distinguish two areas: the contact between the Nazca and the South-America plate that begins at the trench to the down-dip root of the seismogenic zone at approximately 50-60km depth for Northern Chile (Béjar-Pizarro et al., 2010) and the deeper part. To account for the weak resolution in depth of earthquake locations while still isolating each area, we extracted isodepth profiles from SLAB1.0 (Hayes et al., 2012) at 0, 70 and 200km depth in order to build longitudinal boundaries. The catalog is limited in latitude between -18.5N and -22.5N, in accordance with the latitude range of the network. The *interface* catalog contains 7211 (1447 with $M_L \geq 2.1$ for the interface) earthquakes between 0 and 70km slab isodepth, the *intermediate depths* catalog contains 26962 earthquakes (4445 with $M_L \geq 2.6$ for intermediate depths) between 70 and 200km isodepths (Figure 1).

It is important to note that two stations went missing: PB01 from December 5^{th} 2013 to January 1^{st} 2014; PB02 from December 25^{th} 2013 to January 1^{st} 2014. Since the detection capacity of the BackTrackBB method depends on the network coherency (and thus directly on the network geometry), this particular period will be removed from the future analysis.

Examples of the detection-location procedure are displayed in supplementary materials.

3 Declustering of the catalog: Nearest-neighbor distance

Analysis of the background seismicity is a powerful tool to reveal transient deformations (Marsan et al., 2013; Reverso et al., 2015, 2016). Among numerous declustering techniques (Van Stiphout et al., 2012) we selected the nearest-neighbor-distance metric (NND) proposed by (Baiesi & Paczuski, 2004) because it is self-adapted to observed seismicity and does not use tuning parameters other than the characteristic of each event (i.e. the magnitude, the location and occurrence time). It also represents a good compromise between computational efficiency and stabililty of the results. It consists of the estimation of the distance η between each event j and any event i that precedes it. Thus, the nearest-neighbor event will be the event i that minimizes this distance:

$$\eta_{i,j} = t_{i,j}(r_{i,j})^{df} \cdot 10^{-b \cdot m_i} \tag{1}$$

where $t_{i,j} = t_j - t_i$ in days, $r_{i,j} = |r_i - r_j|$ in kilometers, m_i is the parent local magnitude, *df* is the fractal dimension which we set to 2 since we consider that the seismicity is located on the horizontal plane and b from the Gutenberg-Richter law (here $b =$ 0.87, Figure 1). Zaliapin et al. (2008) went further and introduced a re-scaled time-difference $T_{i,j}$ and distance $R_{i,j}$ for discriminating clustered and non-clustered events in order to account for both time and space in the η distribution:

$$\eta_{i,j} = T_{i,j} \times R_{i,j}$$

$$
\begin{aligned}
T_{i,j} &= t_{i,j}.10^{-\frac{1}{2}.b.m_i} \\
R_{i,j} &= (r_{i,j})^{df}.10^{-\frac{1}{2}.b.m_i}
\end{aligned}
\tag{2}
$$

The η distribution of equation 1 of the intermediate-depths catalog is uni-modal (Figure 2) and, following Zaliapin et al. (2008); Zaliapin and Ben-Zion (2013), can be described with a logarithmic scale by a Weibull function. If we consider $x = \log(\eta)$, the Weibull function is:

$$
f(x|x_0, \lambda, k) = \begin{array}{ll} k\lambda \left(\frac{x-x_0}{\lambda}\right)^{(k-1)} \exp\left[-\left(\frac{x-x_0}{\lambda}\right)^k\right] & x \geq x_0 \\ 0 & x < x_0 \end{array}
\tag{3}
$$

Where $k > 0$ is the shape parameter, $\lambda > 0$ is the scale parameter of the distribution and x_0 is the location parameter. We are able to determine the 3 parameters x_0, λ and k, through the minimization of an L2-norm.

The η distribution of the interface catalog is bi-modal (Figure 2) as expected (Zaliapin et al., 2008; Zaliapin & Ben-Zion, 2013). To separate the two populations, we modeled the distribution in this particular case with a sum of a log-Gaussian function, $g(x) = a_0 \exp((x-x_0)/\sigma)$ and a Weibull function (equation 3). We fit the whole distribution by minimizing an L2-norm. We finally determine the threshold between the two population as the local minimum of the Gaussian and the Weibull distribution. This compromise means that we will include a portion of background seismicity into the clustered catalog and a portion of the clustered seismicity into the background catalog.

We clearly identify the three seismic swarms in the interface seismicity as aftershocks. In the following, we will study the background seismicity of the interface and intermediate-depth catalogs to detect spatio-temporal variations of their seismic rate that could be explained by aseismic slip. As suggested we do not consider the background seismicity before February 1^{st} 2013 due to edge-effects: there are no sufficient background earthquakes to identify potential aftershocks. This may lead to an over-estimation of the background seismic rate at the beginning of the catalog and ultimately induce a decrease of the seismic rate as soon as the declustering algorithm is stabilized.

4 Analysis of the background seismicity

4.1 Reference Poisson-law

Siméon-Denis Poisson introduced in 1838 the Poisson-law to express the probability of a given number of events k occurring in a fixed interval of time T if these events occur with a known constant rate T_0 and independently of the time since the last event:

$$
P(k, T, T_0) = \frac{1}{k!}\left(\frac{T}{T_0}\right)^k \exp\left(-\frac{T}{T_0}\right)
\tag{4}
$$

Gardner and Knopoff (1974) demonstrated that a sequence of earthquakes in Southern-California freed from aftershocks follows a Poisson law in time. Recently Marsan et al. (2017) revealed aseismic transients along the Pacific Plate in Japan by comparing an initial background seismic rate to an expected seismic rate. The authors demonstrated that the declustering following a Nearest-Neighbor-Distance Algorithm (Baiesi & Paczuski, 2004; Zaliapin et al., 2008) is consistent with the use of a space-time Epidemic-Type Aftershock-Sequence (ETAS) model (Ogata, 1998), hence is suitable for studying the background seismicity variations through time. Here we won't analyze the clustered seismicity.

4.2 Kolmogorov-Smirnov one-sample test

The Kolmogorov-Smirnov one sample test (**KS1**) is a non-parametric statistical test commonly used to test the equality between a distribution and a reference law through the estimation of a distance between the two (Lehmann & Romano, 2006; Gibbons & Chakraborti, 2011). For the corresponding cumulative distribution functions, the observed distribution $F(x)$ of with a number of sample n and the theoretical distribution $P(x)$, the test consists in the estimation of the Kolmogorov-Smirnov criterion, denoted D_n, which is the maximum of the absolute difference between the two cumulative distribution functions:

$$D_n = \max_x |P(x) - F_n(x)| \tag{5}$$

In seismology, the KS test has been used to assess the uniformity of declustered earthquake catalogs (Reasenberg & Matthews, 1988; Matthews & Reasenberg, 1988) but never to study seismic rate variations. In the following, we won't consider the absolute difference in equation 5 but will keep the information held by the sign of the difference. This will offer an indication of an event deficit (negative sign: F_n exhibits a greater probability for smaller number of event per day in regard to P) or an event excess (positive sign: F_n exhibits a greater probability for greater number of event per day in regard to P). In the following we refer to Dn as the event excess (a negative event excess is an event deficit). The null hypothesis, $H_o : F_n(x) = P(x)$, is considered rejected at significance level α, if:

$$|D_n| > \frac{K(\alpha)}{\sqrt{n}} \tag{6}$$

where $K(\alpha)$ is a constant and its value can be found in tables (Gibbons & Chakraborti, 2011) or can be estimated from the Kolmogorov distribution (Kolmogorov, 1933). In the following we will consider three levels of significance α: $K(\alpha = 0.68\%) = 0.96$, $K(\alpha = 0.95\%) = 1.36$ and $K(\alpha = 0.99\%) = 1.63$.

One cannot assess which period corresponds to the *stable* seismic rate especially for a catalog of this size (473 days). In the following analysis, we simply count the number of earthquakes per day. We consider that a sampling of $T = 1$ day is enough to both have a sufficient number of samples and a sufficient number of events per window. We now attempt to detect any changes in the seismic rate between a reference period that we will call T_{ref} and the period that follows until April 1^{st} 2014.

We begin by fixing T_{ref}: July 23^{rd} 2013, the day of the first cluster prior the Iquique earthquake. We infer an average inter-event time $T_0 = T_{ref}/N_{ref}$, with N_{ref} the total number of events observed during T_{ref} for the interface and intermediate-depth declustered catalogs. We compute the reference-Poisson probability density function , P_{ref} following equation 4. In a similar way, we count the number of earthquakes per day from the end of the reference period until April 1^{st} 2014. We make sure to remove samples comprised in the period of station loss ($n = 282$ remaining sample) to obtain the two earthquake counting distributions $F_{obs}(k)$ (Figure 3).

Next, we tested with a KS1, the null hypothesis $H_0 : P_{ref}(k) = F_{ref}(k)$; put simply, is the theoretical Poisson law P_{ref} significantly similar to the observed distribution F_{ref}?. Using P_{ref} guaranties us to overcome the problem of the reduced number of samples (days) of F_{ref} and rather consider a infinite number of samples with P_{ref}. This test shows that we cannot reject the null hypothesis H_0 and thus confirms that P_{ref} and F_{ref} cannot be distinguished. In the following, we generate the observation counting distributions, F_{obs}, starting from T_{ref}, the time of the first cluster, to March 31^{st} 2014, the day before the mainshock, (Figure 3).

Another KS1 test is performed to evaluate the null hypothesis $H_1 : P_{ref} = F_{obs}$ for both catalogs (Figure 4). The null hypothesis H_1 is rejected for the interface background catalog with a significance of more than 99%, suggesting a great increase of the global seismicity after this date. For the intermediate-depth catalog, we obtain a negative event excess Dn but only significant at 68% which we won't consider sufficient to be interpreted.

4.3 KS1 for a range of reference period date

While the T_{ref}: July 23rd 2013 in the previous section is justified by the initiation of the first cluster in July 2013, it is an arbitrary parameter. We computed the KS1 for a range of T_{ref} from April 1st 2013 until October 1$_{st}$ 2013 with a step of a day. Thus we obtain an event excess Dn for each catalog at each possible T_{ref}. The results are shown in Figure 5. We can observe a general and progressive increase of the event excess also marked by a stronger and more significant acceleration around the July 2013 cluster for the interface catalog while it appears to decrease over time at intermediate-depths towards a more significant deceleration for greater T_{ref}.

Until now we have only considered the full declustered catalogs, without taking the spatial information into account. To have an overview of the spatio-temporal evolution of both interface and intermediate-depths background catalogs we apply the KS1 test at each node of a 2D grid discretized every 5km and consider the events that occurred with a 30km radius of the center of each grid cell.

4.4 Mapping the Kolmogorov-Smirnov one-sample test

This spatial KS1 can be applied for all sub-catalogs and the determined event excess $Dn(x, y|T_{ref})$ are assigned to all specific nodes associated to a longitude x and a latitude y. Based on the previous results of the estimation of the event excess for different reference period, we will consider 2 T_{ref}: T^1_{ref}: May 20th 2013, which is before the largest acceleration for the interface declustered catalog and T^2_{ref}: July 23rd 2013, which is the time of the first cluster.

$\mathbf{T}^1_{ref}$: May 20th 2013

The spatial KS1 for the interface background catalog shows striking patterns (Figure 6a): we observe two offshore patches of event excess with significance over 68%, though only one is 95% significant (see bootstrap distribution for this region in Figure S7 in Supplementary Information). We observe a broad region of event deficit with significance over 99% in the center (see bootstrap distribution for this region in Figure S7 in Supplementary Information). Regarding the intermediate-depths (Figure 7a), the spatial KS1 displays three large regions of event deficit with significance larger than 99% with one located at the latitudes of the Iquique mainshock and its major aftershock.

$\mathbf{T}^2_{ref}$: July 23rd 2013

The spatial KS1 for the interface background catalog shows little patches of event excess with reduced extents for a significance over 95% (Figure 6b). The quiescence previously observed is not significant anymore. Concerning the intermediate-depths catalog (Figure 7b), the spatial KS1 still exhibits strong but narrower patches of nevent deficit at the latitudes of the Iquique mainshock (significance $> 95\%$).

5 Discussion

We investigated a potential large scale destabilization of the plate interface in the North of Chile, as evidenced by significant changes in the background seismicity rates. We built a continuous seismic catalog from December 12th 2012 till March 31st 2014 (Figure 1). The catalog's magnitude frequency distribution is described by a Gutenberg-Richter law with $b = 0.87$ and a completeness magnitude $M_c = 2.6$. We took particular care to select stations for the detection phase in order to avoid a bias in the estimation of the seismic-rate.

We investigated the declustered seismic-rate for two regions: the interface ($z < 70km$) and the intermediate depths ($70km < z < 200km$). After the declustering of both catalogs with the Nearest-Neighbor-Distance algorithm (Baiesi & Paczuski, 2004; Zaliapin et al., 2008; Zaliapin & Ben-Zion, 2013) (Figure 2), we searched for potential transient processes in these declustered catalogs following an original framework based on a one-sample Kolmogorov-Smirnov test. First, we separated each catalog into two periods, the reference period and the observation period, before and after T_{ref}: July 23^{rd} 2013. We then compared both time periods in order to investigate a potential change in the seismic rate (Figure 4). The KS1 test shows that the interface experienced a significant acceleration of seismicity ($>99\%$ of significance) after the first cluster of July 2013 while the seismicity rate at intermediate-depths seems to have remained constant (Figure 4). This first observation is in agreement with several studies that have proposed the unlocking of the plate interface from this period (Schurr et al., 2014; Kato et al., 2016; Socquet et al., 2017).

We then applied the same test for P_{ref} and the observation counting distribution F_{obs} for all possible T_{ref} between April 2013 and October 2013 (Figure 5). This second approach of the KS1 allows to observe a continuous increase of the event excess Dn ($Dn(t+\Delta t) > Dn(t)$)for the interface while it is decreasing for the intermediate-depths ($Dn(t+\Delta t < Dn(t)$). It is difficult to estimate a time scale for this, however the anti-correlation could be explained by a very simplistic hypothesis: before the unlocking of the interface, the slab is dragged at depth by its own weight and the convective motions in the mantle. This generates tensile stress into the slab, which is thought to be the source of the mechanisms of most deep earthquakes (Astiz & Kanamori, 1986; Dmowska & Lovison, 1988). When the interface starts to unlock, the tensile stress will be reduced: as a consequence the seismicity rate may decrease. However, this supposition needs to be confirmed by more in-depth studies. Here, it is not clear when the initiation of the seismic-rate acceleration takes place along the interface and when it starts to decrease at depth.

When we reproduce the KS1 test spatially for two different reference periods, striking patterns come out. It is interesting to note that, for a different T_{ref}, the spatial distribution of event excess Dn can be drastically different (Figures 6 and 7). For the interface and for T_{ref}: July 23^{rd} 2013, we have a regional event excess Dn that overcomes the 99.9% of statistical significance (Figure 5), however the map of spatial Dn for the same period of reference show areas of negative Dn (which are not significant) (Figure 6b). This is not surprising since we would have expected that the regional event excess Dn to represent a spatial average of the region. We thus observe a large area of significant event deficit compensated by regions of significant and positive Dn.

The spatial distribution of event excess and its regional average are not contradictory, providing complementary insights on the background seismicity at two different scales: (1) the level of the subduction itself and (2) at a 30km-scale. Concerning the difference observed between the two spatial KS1 tests (Figure 6 and 7), they do not constitute a paradox; it only demonstrates that this test is powerful to detect anomalies in the seismicity. By changing T_{ref} we moved the anomalies from the observation to the reference period.

With this original framework based on the one-sample Kolmogorov-Smirnov test and parameters relying only on observations, we are able to detect a global acceleration of the interface background seismicity while it decelerates at intermediate depths. We are also able to detect a quiescence down-dip of the Iquique earthquake nucleation area before the first cluster of July 2013 while the seismicity seems to have accelerated in different proportions in the surroundings of the mainshock.

Quiescence has been observed many times before large earthquakes (Wyss & Habermann, 1988; Ogata, 1992; Wiemer & Wyss, 1994; Wu & Chiao, 2006; Katsumata, 2018) but the potential mechanisms that are at the source of this quiescence are still poorly understood. It is interesting to observe that the quiescence appears in a region of high slip deficit (Figure 8) (Métois et al., 2016). This implies that a high-degree of coupling measured over decades (interseismic period) may vary during a certain period and could be rather different when a megathrust earthquake is about to occur (Marsan et al., 2017). However to determine the potential mechanisms between this variations of coupling, we certainly need a precise relocation of the earthquakes from this catalog. Seeking for migrations of seismicity or fluid diffusion evidences (Yoon et al., 2009; Poli, 2017; Pasten-Araya et al., 2018) or repeating earthquakes in the deeper region of the interface may give us clues to improve our understanding of the preparatory phase of the Iquique earthquake.

6 Conclusion

Through the lens of the micro-seismicity, our results confirm the large-scale unlocking of the Iquique interface, expanding from approximately -20.5N to -19.5N. We suggest that the Iquique mainshock may have been triggered by a stress build-up promoted by fluids flows and/or aseismic slip both up-dip and down-dip and/or motion on upper-plate crustal fault(s).

We highlight here the importance of building more complete and detailed catalogs, taking particular care of limiting artifacts which may artificially alter the seismic-rate. Permanent or semi-permanent ocean bottom seismic and geodetic observatories are an absolute necessity for assessing the seismic hazard in subduction zones such as northern Chile. To conclude, the joint use of all geophysical data-sets available is a requirement to improve our understanding of the preparatory phase of megathrust-earthquakes.

Acknowledgments

F.A.A. wants to thank S. Ruiz and M. Bouchon for interesting and constructive discussions and comments. The authors thank everyone who has contributed to the IPOC and ILN network. This is IPGP contribution number XXXX. The seismic catalog created for this study is available here: `https://doi.org/10.5281/zenodo.3597154`.

References

Astiz, L., & Kanamori, H. (1986). Interplate Coupling and Temporal Variation of Mechanisms of Intermediate-depth Eearthquakes in Chile. , *76*(6), 1614–1622.

Baiesi, M., & Paczuski, M. (2004). Scale-free networks of earthquakes and aftershocks. *Physical review E*, *69*(6), 066106.

Bedford, J., Moreno, M., Schurr, B., Bartsch, M., & Oncken, O. (2015). Investigating the final seismic swarm before the Iquique-Pisagua 2014 M<inf>w</inf> 8.1 by comparison of continuous GPS and seismic foreshock data. *Geophys. Res. Lett.*. doi: 10.1002/2015GL063953

Béjar-Pizarro, M., Carrizo, D., Socquet, A., Armijo, R., Barrientos, S., Bondoux, F., ... others (2010). Asperities and barriers on the seismogenic zone in north chile: state-of-the-art after the 2007 m w 7.7 tocopilla earthquake inferred by gps and insar data. *Geophysical Journal International*, *183*(1), 390–406.

Bouchon, M., Durand, V., Marsan, D., Karabulut, H., & Schmittbuhl, J. (2013). The long precursory phase of most large interplate earthquakes. *Nat. Geosci.*. doi: 10.1038/ngeo1770

Cesca, S., Sobiesiak, M., Tassara, A., Olcay, M., Günther, E., Mikulla, S., & T, D. (2009). *The iquique local network and picarray.* GFZ Data Services.

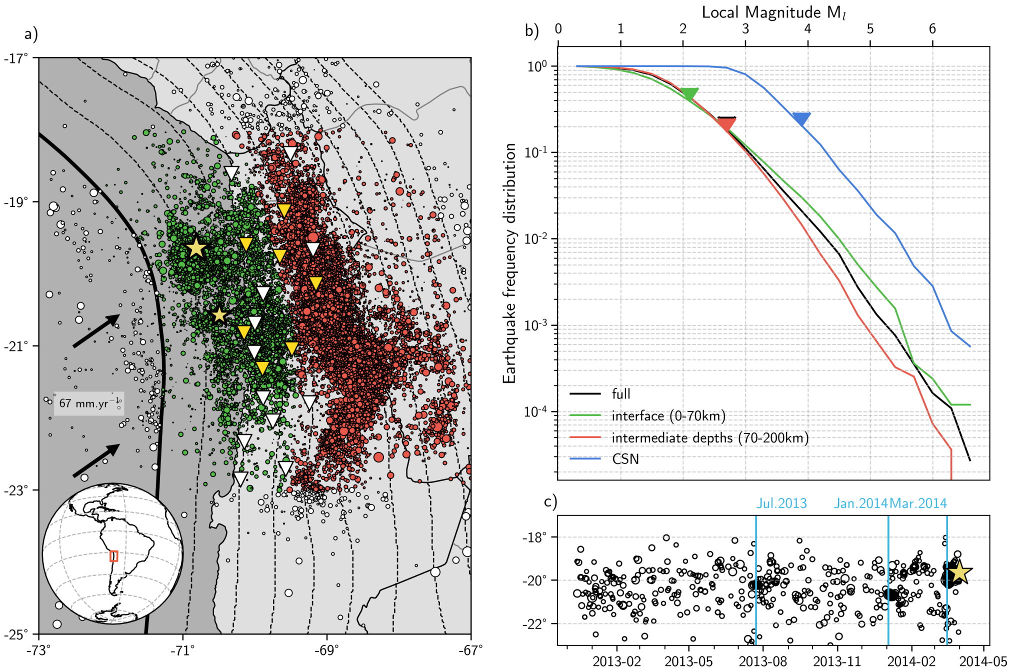

Figure 1. Earthquake catalog for Northern Chile from December 12th 2012 to March 31st 2014. a) Location of the 35371 earthquakes extracted from the IPOC/ILN data-set. The black arrows point the direction of convergence at a rate of 67mm.yr^{-1} vigny2009upper. The solid black line marks the trench separating the Nazca and South-America plates while the dashed lines are the isodepth profile each 20km depth following the Slab 1.0 model hayes2012slab1. The yellow start indicates the location of the Iquique earthquake. The triangle are the stations used in this work, their color indicates if it was used during the detection and location phases (yellow) or location phase only (white). The events are symbolized by circles and their size scale with their local magnitude. Green and red events constitute respectively the interface and the intermediate-depths catalog while white-colored events are discarded for this study. b) Earthquake frequency distribution. Each plain curves correspond to a different earthquake catalog. The completeness magnitude of the presented catalog is 2.6 (CSN $M_c = 3.8$, IPOC $M_c = 2.8$ sippl2018seismicity) with a b-value of 0.87 (CSN $b = 0.85$, IPOC $b = 0.84$). The circles represent the completeness magnitudes of each catalog and the slop of the dashed line are the b-value estimated using a maximum likelihood method. c) Latitude-Time representation of the interface seismicity ($M_l\,3.0^+$) prior to the mainshock. The vertical blue lines mark the three seismic swarms of July 2013, January and March 2014.

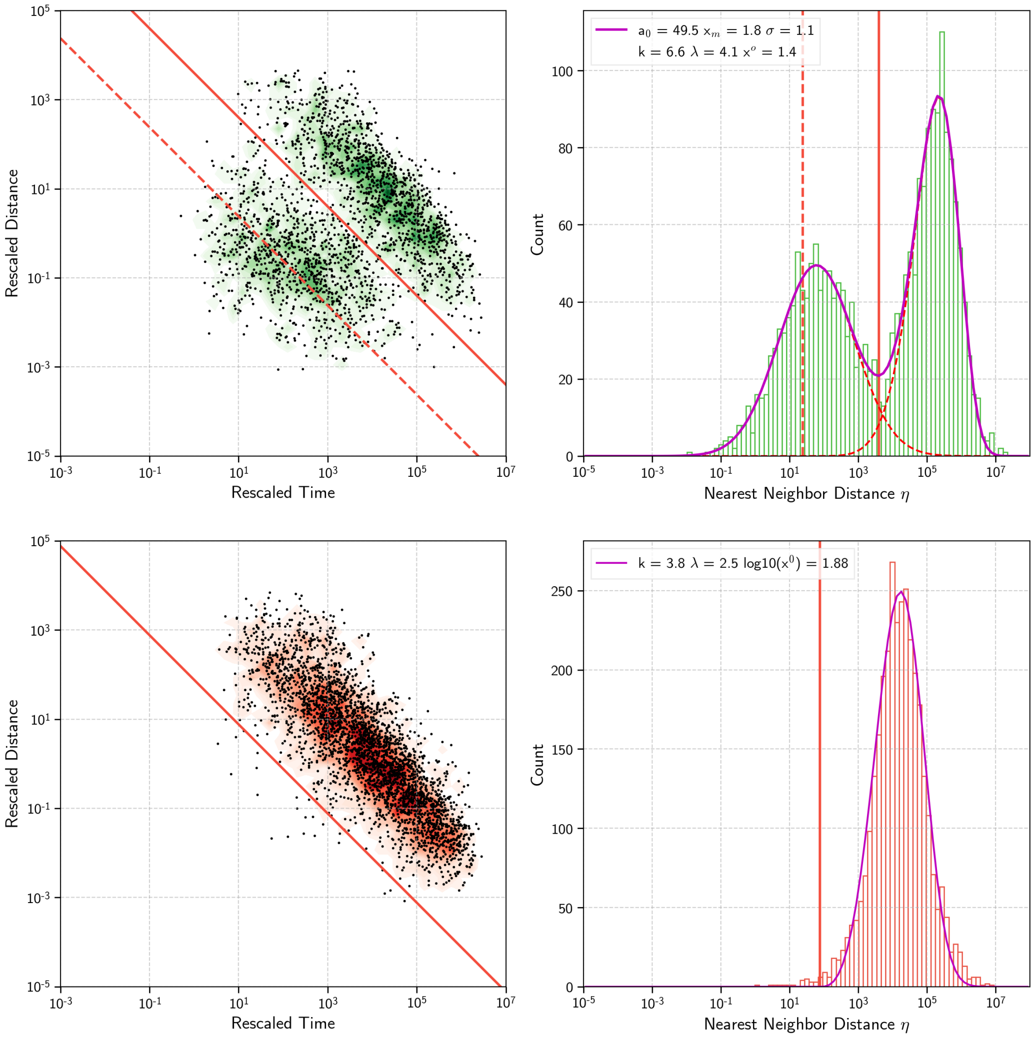

Figure 2. Nearest-Neighbor-Distance applied to the seismicity of Northern Chile. a) Joint distribution of the rescaled time T and distance R of the nearest-neighbor distance η. The intermediate-depths seismicity show a single mode located along the line $\log(R) + \log(T) = 0.86$. b) Histogram of the nearest-neighbor distance η which may be modeled as a log-Weibull function (equation 3). c) and d) stands for the intermediate-depth catalog.

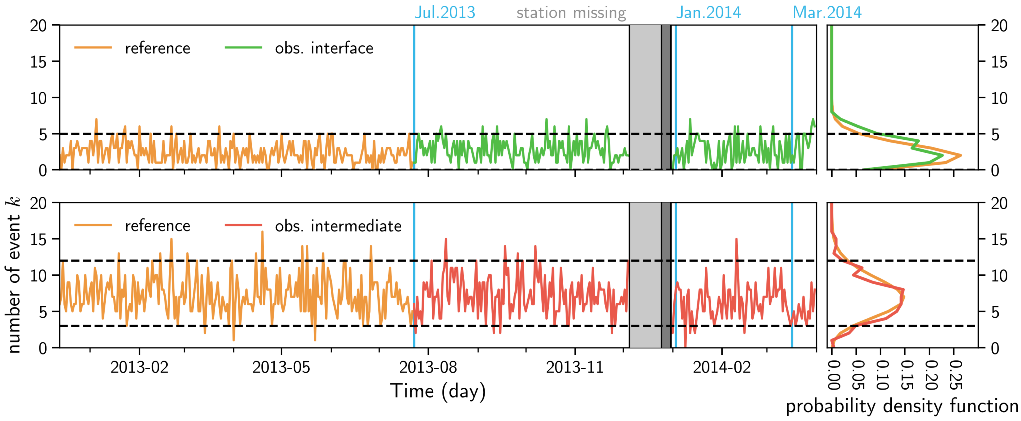

Figure 3. Earthquake counting distributions. a) and c) show the number of earthquake per day, k. This number is orange for the reference period and green (interface) or red (intermediate-depths) for the observation period. The black dashed line correspond to the 95% probability limit of the theoretical Poisson law deduced from the reference period. The vertical blue lines mark the three clusters that preceded the Iquique earthquake, the grey rectangles display the period where two stations of the network went missing. Naturally, the number of earthquakes occurring during these days is not taken into account in the following. b) and d) respectively the probability density function for the observation period of the interface and the intermediate-depths against the theoretical Poisson law.

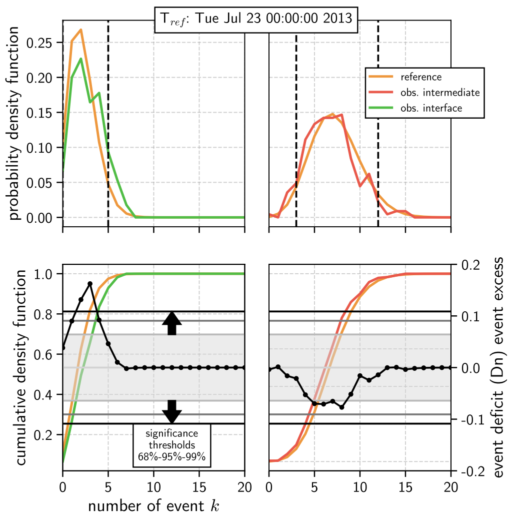

Figure 4. Kolmogorov-Smirnov one-sample test. a) and b) show the probability density functions of the reference (orange) and the observation periods (green and red) for the interface and intermediate-depths background seismicity. The black dashed line correspond to the 95% probability limit of P_{ref}. c) and d) presents the corresponding cumulative density functions. The dotted-black line is the difference between P_{ref} and F_{obs}. The light-grey, dark-grey and black contour lines represents the level of significance respectively at 68%, 95% and 99.9%. For this particular T_{ref}, only the interface background show a Dn at significant level higher than 99.9%, hence rejecting the null hypothesis that both distribution are equivalent.

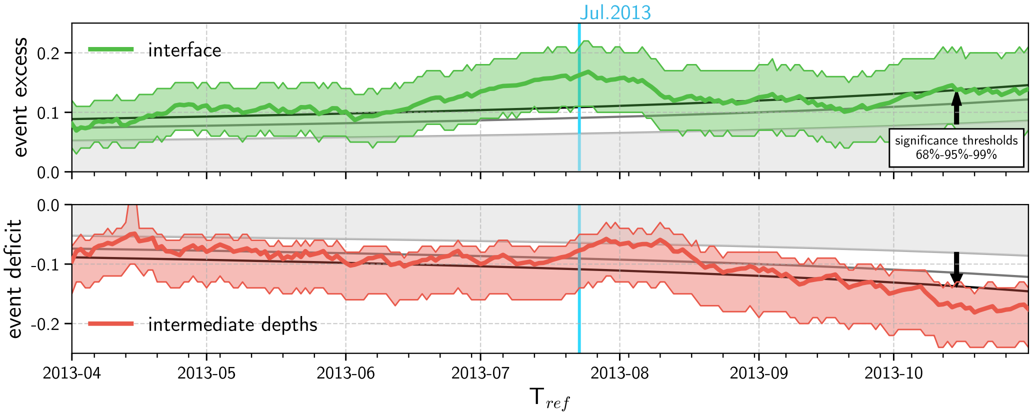

Figure 5. Kolmogorov-Smirnov one-sample test for different reference periods. a) and b) show the evolution of the event excess or deficit Dn by changing T_{ref} respectively for the interface (green) and intermediate-depths (red) background catalogs. The lighter colors represent the 95% confidence intervals estimated by bootstraping (2000 resampling). The light-grey, dark-grey and black contour lines represents the level of significance respectively at 68%, 95% and 99.9% while the grey area represents the region of no significance. The vertical blue line marks the first cluster of July 23^{rd} 2013.

Comte, D., & Pardo, M. (1991). Reappraisal of great historical earthquakes in the northern chile and southern peru seismic gaps. *Natural hazards*, *4*(1), 23–44.

Delouis, B., Nocquet, J.-M., & Vallée, M. (2010). Slip distribution of the february 27, 2010 mw= 8.8 maule earthquake, central chile, from static and high-rate gps, insar, and broadband teleseismic data. *Geophysical Research Letters*, *37*(17).

Dmowska, R., & Lovison, L. C. (1988). Intermediate-term seismic precursors for some coupled subduction zones. *Pure Appl. Geophys. PAGEOPH*. doi: 10.1007/BF00879013

Dorbath, C., Gerbault, M., Carlier, G., & Guiraud, M. (2008). Double seismic zone of the Nazca plate in northern Chile: High-resolution velocity structure, petrological implications, and thermomechanical modeling. *Geochemistry, Geophys. Geosystems*. doi: 10.1029/2008GC002020

Duputel, Z., Jiang, J., Jolivet, R., Simons, M., Rivera, L., Ampuero, J.-P., ... others (2015). The iquique earthquake sequence of april 2014: Bayesian modeling accounting for prediction uncertainty. *Geophysical Research Letters*, *42*(19), 7949–7957.

Gardner, J., & Knopoff, L. (1974). Is the sequence of earthquakes in southern california, with aftershocks removed, poissonian? *Bulletin of the Seismological Society of America*, *64*(5), 1363–1367.

GFZ CNRS-INSU. (2006). *Gfz german research centre for geosciences; institut des sciences de l'univers-centre national de la recherche cnrs-insu (2006): Ipoc seismic network.* Integrated Plate boundary Observatory Chile - IPOC.

Gibbons, J. D., & Chakraborti, S. (2011). Nonparametric statistical inference. In *International encyclopedia of statistical science* (pp. 977–979). Springer.

Hayes, G. P., Wald, D. J., & Johnson, R. L. (2012). Slab1. 0: A three-dimensional model of global subduction zone geometries. *Journal of Geophysical Research: Solid Earth*, *117*(B1).

Huang, H., & Meng, L. (2018). Slow unlocking processes preceding the 2015 mw 8.4

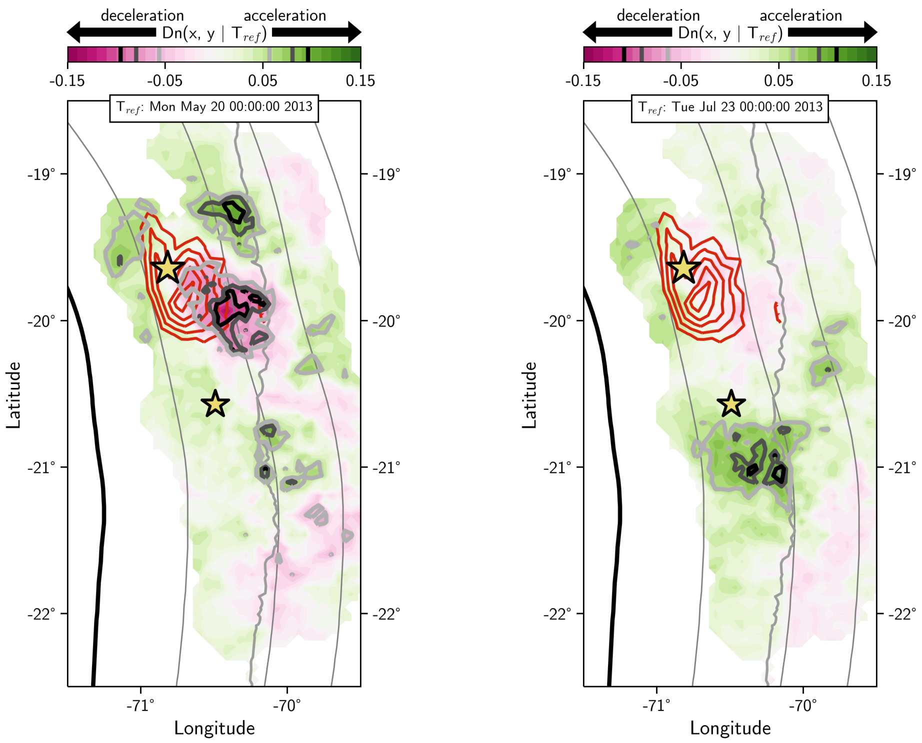

Figure 6. KS1 estimated spatially on the interface background catalog for two reference period: May 20th 2013 and July 23rd 2013. The color-scale represents the local KS1 criterion Dn value from purple (negative) to green (positive). Negative values of Dn are associated to a deceleration of the seismic rate after the time T_{ref} while positive values are related to an acceleration. The light-grey, dark-grey and black contour lines represents the level of significance respectively at 68%, 95% and 99.9%. The red-contour lines represent the slip distribution of the Iquique earthquake. The solid and broad black line is the trench while dashed grey lines are isodepth profiles of the slab at 20, 40, 60 and 80 km deep.

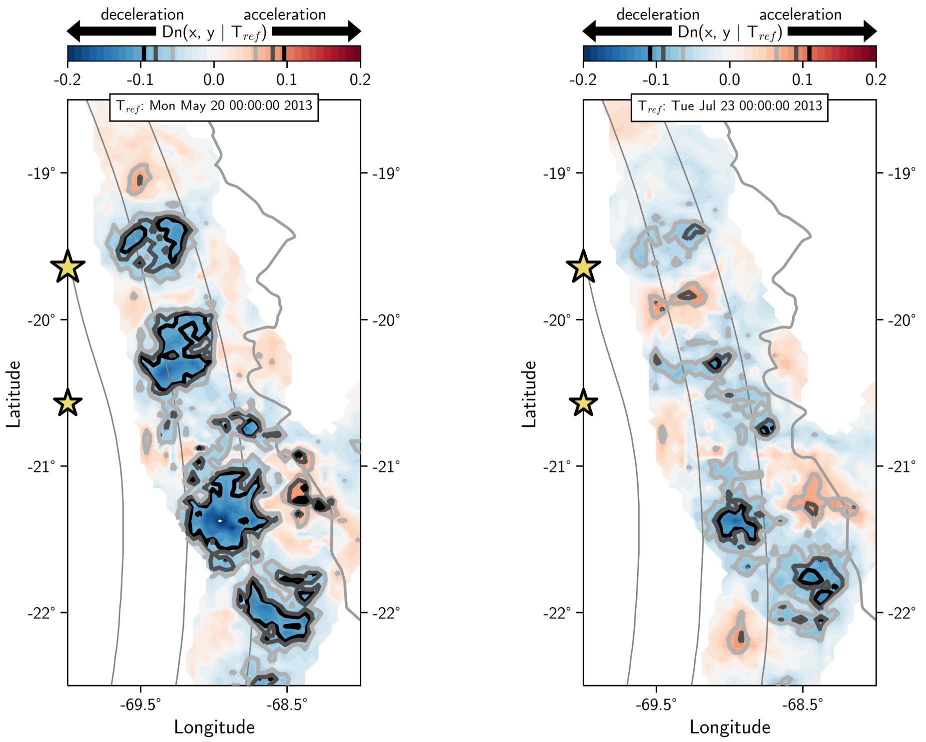

Figure 7. KS1 estimated spatially on the intermediate-depths background catalog for two reference period: May 20th 2013 and July 23rd 2013. The color-scale represents the local KS1 criterion Dn value from blue (negative) to red (positive). Negative values of Dn are associated to a deceleration of the seismic rate after the time T_{ref} while positive values are related to an acceleration. The light-grey, dark-grey and black contour lines represents the level of significance respectively at 68%, 95% and 99.9%. The dashed grey lines are isodepth profiles of the slab at 60, 80 and 100 km deep.

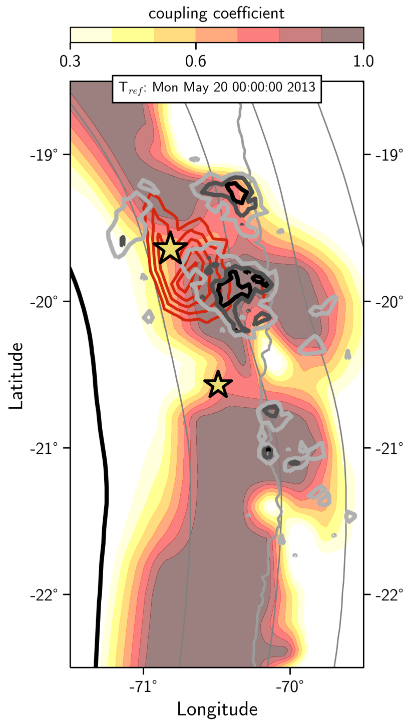

Figure 8. Seismic quiescence and local activation along the interface in relation to the coupling and the Iquique co-seismic slip distribution. The color-scale represents the inter-seismic coupling coefficient (Métois et al., 2016). The light-grey, dark-grey and black contour lines represents the level of significance respectively at 68%, 95% and 99.9% of the event excess and deficit observed in Figures 6 and 7). The dashed grey lines are isodepth profiles of the slab at 20, 40, 60 and 80 km deep.

illapel, chile, earthquake. *Geophysical Research Letters*, *45*(9), 3914–3922.
Jara, J., Sánchez-Reyes, H., Socquet, A., Cotton, F., Virieux, J., Maksymowicz, A., ... others (2018). Kinematic study of iquique 2014 mw 8.1 earthquake: Understanding the segmentation of the seismogenic zone. *Earth and Planetary Science Letters*, *503*, 131–143.
Jara, J., Socquet, A., Marsan, D., & Bouchon, M. (2017). Long-Term Interactions Between Intermediate Depth and Shallow Seismicity in North Chile Subduction Zone. *Geophys. Res. Lett.*. doi: 10.1002/2017GL075029
Kato, A., Fukuda, J., Kumazawa, T., & Nakagawa, S. (2016). Accelerated nucleation of the 2014 iquique, chile mw 8.2 earthquake. *Scientific reports*, *6*, 24792.
Kato, A., Obara, K., Igarashi, T., Tsuruoka, H., Nakagawa, S., & Hirata, N. (2012). Propagation of slow slip leading up to the 2011 mw 9.0 tohoku-oki earthquake. *Science*, 1215141.
Katsumata, K. (2018). Long-term seismic quiescences and great earthquakes in and around the japan subduction zone between 1975 and 2012. In *Earthquakes and multi-hazards around the pacific rim, vol. i* (pp. 233–248). Springer.
Kolmogorov, A. (1933). Sulla determinazione empirica di una legge di distribuzione, giornalo dell'istituto italiano degli attuari 4, 461 (1933). translated in an shiryayev. *Selected Works of AN Kolmogorov*, *2*.
Lay, T., Yue, H., Brodsky, E. E., & An, C. (2014). The 1 april 2014 iquique, chile, mw 8.1 earthquake rupture sequence. *Geophysical Research Letters*, *41*(11), 3818–3825.
Lehmann, E. L., & Romano, J. P. (2006). *Testing statistical hypotheses.* Springer Science & Business Media.
Liu, C., Zheng, Y., Wang, R., & Xiong, X. (2015). Kinematic rupture process of the 2014 chile m w 8.1 earthquake constrained by strong-motion, gps static offsets and teleseismic data. *Geophysical Journal International*, *202*(2), 1137–1145.
Lomax, A. (2005). A reanalysis of the hypocentral location and related observations for the great 1906 california earthquake. *Bulletin of the Seismological Society of America*, *95*(3), 861–877.
Lomax, A., Virieux, J., Volant, P., & Berge-Thierry, C. (2000). Probabilistic earthquake location in 3d and layered models. In *Advances in seismic event location* (pp. 101–134). Springer.
Marsan, D., Bouchon, M., Gardonio, B., Perfettini, H., Socquet, A., & Enescu, B. (2017). Change in seismicity along the japan trench, 1990–2011, and its relationship with seismic coupling. *Journal of Geophysical Research: Solid Earth*, *122*(6), 4645–4659.
Marsan, D., Prono, E., & Helmstetter, A. (2013). Monitoring aseismic forcing in fault zones using earthquake time series. *Bull. Seismol. Soc. Am.*. doi: 10.1785/0120110304
Matthews, M. V., & Reasenberg, P. A. (1988). Statistical methods for investigating quiescence and other temporal seismicity patterns. *Pure and Applied Geophysics*, *126*(2-4), 357–372.
Mavrommatis, A. P., Segall, P., & Johnson, K. M. (2014). A decadal-scale deformation transient prior to the 2011 mw 9.0 tohoku-oki earthquake. *Geophysical Research Letters*, *41*(13), 4486–4494.
Meng, L., Huang, H., Bürgmann, R., Ampuero, J. P., & Strader, A. (2015). Dual megathrust slip behaviors of the 2014 iquique earthquake sequence. *Earth and Planetary Science Letters*, *411*, 177–187.
Métois, M., Vigny, C., & Socquet, A. (2016). Interseismic Coupling, Megathrust Earthquakes and Seismic Swarms Along the Chilean Subduction Zone (38–18S). *Pure Appl. Geophys.*.
Nishenko, S. P. (1991). Circum-pacific seismic potential: 1989–1999. *Pure and applied geophysics*, *135*(2), 169–259.
Ogata, Y. (1992). Detection of precursory relative quiescence before great earth-

quakes through a statistical model. *Journal of Geophysical Research: Solid Earth*, *97*(B13), 19845–19871.

Ogata, Y. (1998). Space-time point-process models for earthquake occurrences. *Annals of the Institute of Statistical Mathematics*, *50*(2), 379–402.

Pasten-Araya, F., Salazar, P., Ruiz, S., Rivera, E., Potin, B., Maksymowicz, A., ... others (2018). Fluids along the plate interface influencing the frictional regime of the chilean subduction zone, northern chile. *Geophysical Research Letters*, *45*(19), 10–378.

Peyrat, S., Campos, J., De Chabalier, J.-B., Perez, A., Bonvalot, S., Bouin, M.-P., ... others (2006). Tarapacá intermediate-depth earthquake (mw 7.7, 2005, northern chile): A slab-pull event with horizontal fault plane constrained from seismologic and geodetic observations. *Geophysical Research Letters*, *33*(22).

Poiata, N., Satriano, C., Vilotte, J. P., Bernard, P., & Obara, K. (2016). Multiband array detection and location of seismic sources recorded by dense seismic networks. *Geophys. J. Int.*. doi: 10.1093/gji/ggw071

Poiata, N., Vilotte, J.-P., Bernard, P., Satriano, C., & Obara, K. (2018, feb). Imaging different components of a tectonic tremor sequence in southwestern japan using an automatic statistical detection and location method. *Geophysical Journal International*, *213*(3), 2193–2213. Retrieved from `https://doi.org/10.1093/gji/ggy070` doi: 10.1093/gji/ggy070

Poli, P. (2017). Creep and slip: Seismic precursors to the nuugaatsiaq landslide (greenland). *Geophysical Research Letters*, *44*(17), 8832–8836.

Poli, P., Jeria, A. M., & Ruiz, S. (2017). The mw 8.3 illapel earthquake (chile): Preseismic and postseismic activity associated with hydrated slab structures. *Geology*, *45*(3), 247–250.

Reasenberg, P. A., & Matthews, M. V. (1988). Precursory seismic quiescence: a preliminary assessment of the hypothesis. *pure and applied geophysics*, *126*(2-4), 373–406.

Reverso, T., Marsan, D., & Helmstetter, A. (2015). Detection and characterization of transient forcing episodes affecting earthquake activity in the aleutian arc system. *Earth and Planetary Science Letters*, *412*, 25–34.

Reverso, T., Marsan, D., Helmstetter, A., & Enescu, B. (2016). Background seismicity in boso peninsula, japan: Long-term acceleration, and relationship with slow slip events. *Geophysical Research Letters*, *43*(11), 5671–5679.

Rosenberger, A. (2010). Real-time ground-motion analysis: distinguishing p and s arrivals in a noisy environment. *Bulletin of the Seismological Society of America*, *100*(3), 1252–1262.

Ruegg, J., Olcay, M., & Lazo, D. (2001). Co-, post-and pre (?)-seismic displacements associated with the mw 8.4 southern peru earthquake of 23 june 2001 from continuous gps measurements. *Seismological Research Letters*, *72*(6), 673–678.

Ruiz, S., Aden-Antoniow, F., Baez, J., Otarola, C., Potin, B., Campo, F., ... others (2017). Nucleation phase and dynamic inversion of the mw 6.9 valparaíso 2017 earthquake in central chile. *Geophysical Research Letters*, *44*(20).

Ruiz, S., Metois, M., Fuenzalida, A., Ruiz, J., Leyton, F., Grandin, R., ... Campos, J. (2014). Intense foreshocks and a slow slip event preceded the 2014 Iquique Mw8.1 earthquake. *Science*. doi: 10.1126/science.1256074

Schurr, B., Asch, G., Hainzl, S., Bedford, J., Hoechner, A., Palo, M., ... others (2014). Gradual unlocking of plate boundary controlled initiation of the 2014 iquique earthquake. *Nature*, *512*(7514), 299.

Socquet, A., Valdes, J. P., Jara, J., Cotton, F., Walpersdorf, A., Cotte, N., ... Norabuena, E. (2017). An 8 month slow slip event triggers progressive nucleation of the 2014 Chile megathrust. *Geophys. Res. Lett.*. doi: 10.1002/2017GL073023

Van Stiphout, T., Zhuang, J., Marsan, D., Stiphout, V., Zhuang, J., & Marsan, D. (2012). Theme V-Models and Techniques for Analyzing Seismicity Seismicity

Declustering. *CORSSA*. doi: 10.5078/corssa

Vigny, C., Socquet, A., Peyrat, S., Ruegg, J.-C., Métois, M., Madariaga, R., … others (2011). The 2010 mw 8.8 maule megathrust earthquake of central chile, monitored by gps. *Science*, *332*(6036), 1417–1421.

Wiemer, S., & Wyss, M. (1994). Seismic quiescence before the landers (m= 7.5) and big bear (m= 6.5) 1992 earthquakes. *Bulletin of the Seismological Society of America*, *84*(3), 900–916.

Wu, Y.-M., & Chiao, L.-Y. (2006). Seismic quiescence before the 1999 chi-chi, taiwan, m w 7.6 earthquake. *Bulletin of the Seismological Society of America*, *96*(1), 321–327.

Wyss, M., & Habermann, R. E. (1988). Precursory seismic quiescence. *Pure and applied geophysics*, *126*(2-4), 319–332.

Yagi, Y., Okuwaki, R., Enescu, B., Hirano, S., Yamagami, Y., Endo, S., & Komoro, T. (2014). Rupture process of the 2014 iquique chile earthquake in relation with the foreshock activity. *Geophysical Research Letters*, *41*(12), 4201–4206.

Yokota, Y., & Koketsu, K. (2015). A very long-term transient event preceding the 2011 tohoku earthquake. *Nature communications*, *6*, 5934.

Yoon, M., Buske, S., Shapiro, S., & Wigger, P. (2009). Reflection image spectroscopy across the andean subduction zone. *Tectonophysics*, *472*(1-4), 51–61.

Zaliapin, I., & Ben-Zion, Y. (2013). Earthquake clusters in southern California I: Identification and stability. *J. Geophys. Res. Solid Earth*. doi: 10.1002/jgrb.50179

Zaliapin, I., Gabrielov, A., Keilis-Borok, V., & Wong, H. (2008). Clustering analysis of seismicity and aftershock identification. *Physical review letters*, *101*(1), 018501.